IEEE Access
Multidisciplinary ⋮ Rapid Review ⋮ Open Access Journal

Received 3 December 2023, accepted 7 December 2023, date of publication 18 December 2023,
date of current version 22 December 2023.

Digital Object Identifier 10.1109/ACCESS.2023.3343707

RESEARCH ARTICLE

A Kruppa Equation-Based Virtual Reconstruction Method for 3D Images Under Visual Communication Scenes

QI YANG[1] AND JONG HOON YANG[2]
[1]School of Journalism and Media, Chongqing Normal University, Chongqing 401331, China
[2]Department of Digital Image, Sangmyung University, Seoul 03016, South Korea

Corresponding author: Qi Yang (whaleyang@163.com)

This work was supported by the Project of Chongqing Normal University under Grant 22XWB017.

ABSTRACT Visual communication (VC) manages to demonstrate optimal perception effect through reasonable element planning. It has been a more prevalent tendency to introduce 3D image reconstruction into VC activities. Currently, there still lacks reliable solution for this purpose under VC scenes. To deal with this issue, we propose a Kruppa equation-based virtual reconstruction method for 3D images under VC scenes. Firstly, the feature descriptor procedure in scale-invariant feature transform (SIFT) algorithm is introduced into image matching. Then, Harris corner extraction (HCE) algorithm is utilized for selection of feature points. And according to HCE algorithm, we develop a specific direction feature description method. In the proposal, main camera points are calibrated separately, which not only makes the calibration accuracy of the main points higher, but also reduces the unknown parameters of Kruppa equation. Finally, we conduct some experiments to verify efficiency of the proposal. The obtained results show that calibration accuracy of the proposal is 12% higher than other comparison methods, and better virtual reconstruction results can be achieved.

INDEX TERMS Kruppa equation, 3D virtual reconstruction, image processing, feature point selection.

I. INTRODUCTION

The Kruppa equation is a mathematical model that describes the laws of visual perception, developed by Czech mathematician Anton í n Kruppa was proposed in the mid-20th century. This equation mainly describes the relationship between the projection of an object on a two-dimensional image plane and the structure of the object itself. Simply put, the Kruppa equation can be used to describe the projection deformation of three-dimensional objects on a two-dimensional image plane, which is caused by factors such as observation angle and light conditions.

The Kruppa equation has a wide range of applications in visual communication scenarios. For example, in fields such as computer vision, image processing, and 3D reconstruction, we need to restore 3D structures from 2D images. At this point, the Kruppa equation can be used to describe the projection deformation of the object surface in the image, thereby helping us recover the three-dimensional shape of the object from the image. In addition, the Kruppa equation can also be used in fields such as virtual reality, augmented reality, and visualization, such as creating realistic 3D scenes and objects in virtual environments.

3D image virtual reconstruction (VR) is a method to obtain the shape information of 3D objects by digital processing technology based on the image information collected from the outside of 3D objects [1]. Virtual reality includes electronic information technology, computer technology and simulation technology, etc. It mainly uses computer simulation environment to make people feel immersed. With the development of science and technology, it has gradually become an independent field of science and technology [2]. Most of the traditional reconstruction methods are in the form of modeling calculation [3]. Although this method can quickly

The associate editor coordinating the review of this manuscript and approving it for publication was Senthil Kumar.

model, the modeling effect of artistic images is not ideal, even vague, which is a kind of destruction to the artistic images themselves [4].

The motivation for using the Kruppa equation is to solve the three-dimensional reconstruction problem in visual communication scenes [23]. In visual communication scenarios, we often need to recover three-dimensional information from two-dimensional images in order to achieve more realistic and vivid virtual environments or visualization effects [24]. However, recovering three-dimensional information from two-dimensional images is a very difficult problem, as many factors are involved in this process, such as lighting conditions, observation angles, texture and shape of the object surface, etc [25]. The proposal of the Kruppa equation provides an effective method for solving this problem [26]. It describes the relationship between the projection of an object on a two-dimensional image plane and the structure of the object itself, which can help us understand and predict the projection deformation of the object in the image [27]. By utilizing the Kruppa equation, we can recover more accurate three-dimensional information from images, thereby creating more realistic virtual environments and visualization effects [28].

With the development of image information processing technology, the requirements for imaging and visual expression of images are increasing [5]. Combining the detailed feature recognition with the optimized detection method, the VR method of regional 3D image, which studies the VC(visual communication) effect, has practical value in image recognition [6]. Communication of content through visual language can enable people of different regions, genders, ages and skin colors to accomplish cultural communication, emotional communication and information transmission through visual and media means [7], [8].

The existing 3D image virtual reconstruction methods often have some problems. For example, many methods have high requirements for the number, quality, and lighting conditions of input images, and their processing capabilities for complex scenes and dynamic objects are also limited. In addition, some methods may produce unrealistic visual effects during the reconstruction process, such as ''edge effects'' and ''visual distortion'', which limit the practical application of 3D image virtual reconstruction technology. In response to these issues, this article proposes a virtual reconstruction method for 3D images based on the Kruppa equation. The innovation contributions are as follows:

1. This method utilizes the Kruppa equation in the field of computer vision and can achieve accurate 3D reconstruction with only a small amount of input images.

2. Due to the strong robustness of the Kruppa equation to changes in lighting and object motion, this method can also effectively handle complex scenes and dynamic objects.

3. By making reasonable use of the properties of the Kruppa equation, this method can also overcome the problems of ''edge effects'' and ''visual distortion'' to a certain extent, and improve the visual effect of reconstruction.

II. RELATED WORK

Clark et al. put forward a normalized convolution method based on spectral fidelity constraint, which takes the spectral correlation between pixels in the local neighborhood of the image as a constraint condition, so as to improve the preservation degree of spectral characteristics of the reconstructed hyperspectral image [9]. László et al. made a detailed study on the evolution of 2D animation and 3D animation in VC, and verified the feasibility and applicability of VC principle in 3D graphic design [10]. Liu et al. calculated the view similarity values of all view pairs, sorted all unordered views into clusters of related views, reconstructed the missing matching between views, and achieved efficient feature matching between unordered views [11].

Tang et al. proposed a method of estimating the basic matrix from point correspondence, and provided a more accurate estimation of the basic matrix by using semi-definite programming to avoid local minimum [12]. Wong et al. simplified the original Kruppa equation by using the singular value decomposition form of basic matrix [13]. Karam et al. analyzed Krupp equation in detail, and pointed out that in some special cases, such as when the camera moves in pure rotation or translation, Krupp equation can be transformed into a linear equation [14]. Li et al. researched and developed a set of automatic 3D surface generation system, which adopted the camera self-calibration method with variable parameters [15]. Xia et al. studied how to reconstruct the 3D space model of the image target object from the image sequence when the image is obtained without calibration, that is, when the parameters in the camera are unknown [16].

Image processing technology is widely used in various fields. With the support of computer processing technology, the optimization of images can be realized [17], [18]. VC conveys the designer's works to the audience through visual media, which can reflect the characteristics of the times and rich connotations of the works. Visual symbols are used to convey all kinds of information, and the purpose of communication is achieved by ''watching''. Therefore, this paper puts forward an algorithm of 3D image VR based on kruppa equation to quantify the infectivity of VC, which can improve the user experience and the efficiency of human-computer interaction.

III. RESEARCH METHOD

A. VISUAL COGNITIVE ANALYSIS OF 3D GRAPHICAL USER INTERFACE

People's visual behavior is not only a simple physiological activity behavior, but also a psychological behavior, which needs to watch the thinking activity of the subject. Therefore, in the VR of 3D images, attention should be paid to the process of stereoscopic imaging, that is, people's visual organs are two eyes, and the distance will lead to different 3D perception experiences [19].

Psychological research proves that attention includes two aspects: purpose-oriented selection and stimulus-driven

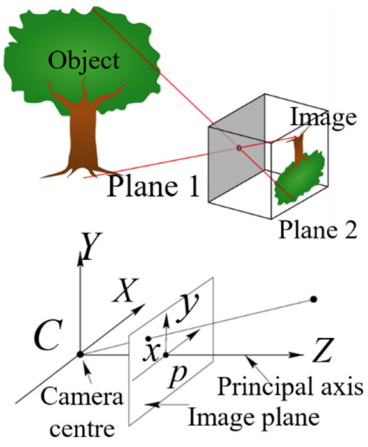

FIGURE 1. Pinhole model.

capture. Purpose-oriented selection is active attention, while stimulus-driven capture is passive attention. For example, in a static graphical user interface, it is easy to attract visual attention if dynamic 3D graphics suddenly jump out. The 3D graphical user interface is composed of static 2D graphics and dynamic 3D graphics. This dynamic and static contrast, 3D and 2D visual differences, make users pay more attention to the interface. The 3D graphical user interface often uses memory fragments in the user's brain to awaken the user's unconscious memory, repeatedly conducting visual stimulation, so that the visual fragments in the brain can evolve into visual symbols. When seeing similar visual elements, it is easy to have a feeling of knowing each other.

The camera imaging process is the process that an object is projected from 3D space to 2D plane. Only by determining the projection model of the camera can the relationship between 3D space points and their projection on 2D image plane be determined. Its view is similar to a pyramid with its top and bottom cut off. Projection is usually used in animation, visual simulation and many other aspects with realistic reflection. Imaging can be divided into three processes, namely, the conversion from world coordinate system to camera coordinate system, from camera coordinate system to image coordinate system and from image coordinate system to pixel coordinate system.

Camera calibration is an indispensable step to obtain 3D information from 2D images. The camera parameters are always relative to some geometric imaging model, which simplifies the optical imaging process. Pinhole model is a perspective projection model of camera. The pinhole model of the camera is shown in Figure 1. A hole is punched in the first plane, through which the light emitted and reflected by the object forms an inverted image on the second plane. The plane 1 is the focal plane, the plane 2 is the image plane, and the pinhole is the optical center [20].

Because the world coordinate system is the coordinate system we take in the natural environment, we can take it to be consistent with the camera coordinate system of the first picture, or the conversion from the world coordinate system to the camera coordinate system can be expressed as follows:

$$\begin{bmatrix} X_c \\ Y_c \\ Z_c \\ 1 \end{bmatrix} = \begin{bmatrix} R & t \\ 0^T & 1 \end{bmatrix} \begin{bmatrix} X_w \\ Y_w \\ Z_w \\ 1 \end{bmatrix}, \tag{1}$$

3D projective transformation is a reversible homogeneous linear transformation in projective space. This transformation can be described by the 4×4 matrix H in formula (2):

$$X' = HX, \tag{2}$$

where H matrix is called projective transformation matrix or homography matrix.

In projective space, if we know this infinite plane π'_∞ which is transformed by projective transformation, we can get the original standard infinite plane by an inverse transformation, so that we can get the transition from projective space to affine space accordingly. The inverse transformation is deduced as follows:

$$T^{-T}\pi'_\infty \cong [0,0,0,1]^T \rightarrow T^T [0,0,0,1] \cong \pi'_\infty, \tag{3}$$

it can be concluded that the last row of the transformation matrix T is equal to π'_∞.

If the fourth element of π'_∞ is normalized to, the transformation matrix T can be selected as the following simple form:

$$T = \begin{bmatrix} I_{33} & 0 \\ \pi'_\infty & 1 \end{bmatrix}, \tag{4}$$

let the coordinates of the space point in the world coordinate system and the camera coordinate system be:

$$X_W = (x_w, y_w, z_w, 1)^T, \tag{5}$$

$$X_C = (x_c, y_c, z_c, 1)^T. \tag{6}$$

The relationship between them is:

$$X_C = \begin{bmatrix} R & -R\tilde{C} \\ 0^T & 1 \end{bmatrix} X_W, \tag{7}$$

where $\tilde{C}$ is the non-homogeneous coordinate of the camera center in the world coordinate system.

B. 3D IMAGE VR

Deep learning has attracted increasing attention in the field of tomographic image reconstruction, especially in the fields of CT, MRI, PET/SPECT, ultrasound, and optical imaging. Sparse view CT remains a challenge among various topics, with the goal of reconstructing decent images from very few projections. The optimization network based on dual domain residuals has advantages in edge preservation, feature restoration, and reconstruction accuracy in preclinical and clinical settings [21]. The only visual appearance is color and brightness [29]. The contour line is inferred from the brightness and color of the eyes in different areas. Light and shadow are the important conditions to form a three-dimensional shape, and these two conditions complement

each other with color and brightness [30]. The production of color perception involves three elements and their relationship. These three elements are light, various materials and the nature of eyes. Besides light and the surface texture of objects, eyes are the last element to make color vision a reality [31]. Cone cells are not stimulated by only one color, but they are stimulated by this color the most, and they are stimulated by the other two colors weakly. For example, pure red light energy strongly stimulates the receptors sensitive to red light, while the stimulation of the other two kinds of light is relatively weak, so people have red vision.

Computer graphics and images are used to visually convey the design, attract consumers' attention, and show a variety of food packaging, clothing, packaging and other works. Whether it's the traditional data, or the electronic posters, publicity color pages and so on, the richness of VC is realized through computer graphic design software. In the 3D image VR system, the input image should be analyzed first, including data input, file analysis and image display. Then, the original 2D data is preprocessed to transform the plane image into a 3D image. Establish an independent relationship among the modules of the system, which is convenient for the maintenance and expansion of the system and ensures that users have a good experience.

The texture gradient decomposition is carried out, and the texture distribution set of the fuzzy regional 3D image is calculated as follows:

$$w(i,j) = \frac{1}{Z(i)} \exp\left(-\frac{d(i,j)}{h^2}\right), \tag{8}$$

where $Z(i)$ is the first-order and second-order texture distribution operators.

After effective calculation, the pixel can realize the parameter analysis of VC constraint, and in order to simplify the calculation process, the relevant parameters are replaced and converted into:

$$W' = \frac{1}{2} f\left(x', y', z'\right) + E, \tag{9}$$

where: x', y', z' is the 3D coordinate value with visual constraint; E represents the weighted component of data, and the matching effect can be directly calculated by formula conversion.

Its visual elements are mainly composed of display visual elements and control visual elements, as shown in Figure 2. Applying VC technology to VR, users send out operation signals through intelligent terminals, which are processed and stored in the system, and the visual elements are fed back to 3D images. The design of 3D image VR system is completed by user feedback information data.

The Fractional Based Generation Model (SGM) has shown significant performance in solving challenging underdetermined inverse problems in medical imaging. However, obtaining high-quality training datasets for these models remains a challenging task, especially in medical image reconstruction. The common noise disturbances or artifacts in low-dose computed tomography (CT) or undersampling

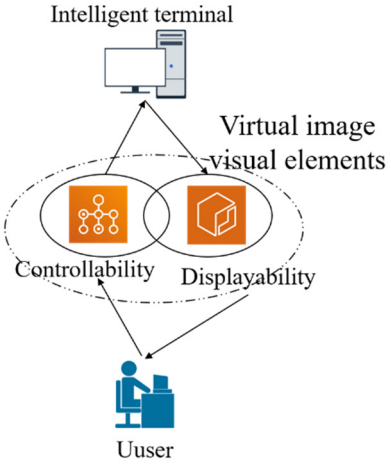

FIGURE 2. Virtual image visual interaction process.

magnetic resonance imaging (MRI) hinder the accurate estimation of data distribution gradients. This affects the overall performance of SGM when using these data for training [22]. LM (Levenberg-Marquardt) optimization algorithm is a commonly used nonlinear least square method, which combines the respective advantages of steepest descent method and Gaussian Newton method [32]. In one iteration of the algorithm, when the obtained solution deviates far from the optimal solution, the algorithm can be approximately regarded as the steepest descent method [33]. When the obtained solution deviates from the optimal solution, the algorithm can be approximately regarded as the steepest descent method. When the obtained solution deviates from the optimal solution, the algorithm can be approximately regarded as Gaussian Newton method.

If there are vectors $a_1, \cdots, a_n$, connecting them together can get $\left(a_1^T, \cdots, a_1^T\right)$, and the optimization problem for 3D reconstruction can be written as the following formula:

$$\min \sum_{k=1}^{m} \sum_{i=1}^{n} D\left(m_{ki}, P_k M_i\right)^2. \tag{10}$$

In this formula, k represents the number of photos taken at different positions, with a total of m images, i represents the serial number of 3D points, with n 3D coordinate points in total, P_k represents the projection matrix of the k-th image, M_i represents the coordinates of the i-th 3D point, $P_k M_i$ represents the calculated 3D coordinates multiplied by the projection matrix and projected back into the image coordinate system, and m_{ki} represents the two-dimensional coordinates of the i-th 3D point on the k images. The whole formula represents the sum of squares to minimize the projection error.

This description uses the difference of two kinds of Gaussian distributions to describe their proximity, and accurately describes the merging rules.

$$J_{merge}\left(i,j;\Theta^*\right) = \left(P_i\left(\Theta^*\right) - P_j\left(\Theta^*\right)\right)^T * \left(P_i\left(\Theta^*\right) - P_j\left(\Theta^*\right)\right), \tag{11}$$

among, the smaller $J_{merge}(i, j; \Theta^*)$ is, the closer the two Gaussian distributions are, and they can be merged.

C. QUANTITATIVE DATA PROCESSING OF APPEAL IN VC

The concept principle of 3D graphic user is set based on the user's psychological model. It is necessary to set the user to be a smart and busy person, so as to avoid the vague concept in operation. Don't let users perform complicated and uncertain information tasks. In the process of 3D interface switching, users' acceptance of dynamic frequency should be considered. In the process of drawing a graph, users often change the position and volume of the graph, and the numerical value in the numerical column at the top of the page will change accordingly, instead of jumping out of the dialog box to remind the user, which saves the user's operation time, improves the operation efficiency, and enables the user to have direct interaction with the interface.

For example, the navigation and window forms in the 2D interface have formed an established pattern in the user concept, so its operation mode should be kept in the 3D user interface design, and only its reasonable integration and application in the 3D environment should be considered. The functions used by more users should be highlighted, so that users can quickly and effectively locate and input them. The actual coordinate of the object is different from the coordinate value we got at present by one scale, rotation and translation information, and there are seven similar transformation matrices with unknown parameters. In the traditional field of photogrammetry, the solution to this problem is often to deal with this nonlinear optimization problem through the process of continuous iteration and gradual refinement. It is necessary to design the iterative process according to the specific problem-giving conditions.

If the design is good, satisfactory results can often be obtained after several cycles. Therefore, this is a practical method, which can solve some difficult problems that can't be illustrated. Although the accuracy of drawing can't be very high, it can provide initial value for mathematical iterative method. Well helps to judge the convergence of the iterative formula. Different from the existing algorithms, this algorithm calibrates the main points of the camera separately, which not only makes the calibration accuracy of the main points higher, but also reduces the unknown parameters of Kruppa equation and improves the accuracy of the final calibration result.

The basic matrix can be deduced from the epipolar geometry constraints outside the two views:

$$F = \alpha\left(e'\right) \times KPK^{-1}, \tag{12}$$

where e is the pole on the second image, and following formula is obtained:

$$\left[e'\right] = \begin{bmatrix} 0 & -e_3 & e_2 \\ e_3 & 0 & -e_1 \\ -e_2 & e_1 & 0 \end{bmatrix}. \tag{13}$$

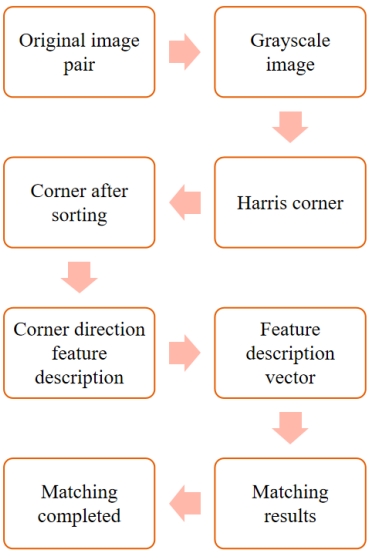

FIGURE 3. Matching method flow chart.

Let $\mu = \alpha^2, C = KK^T$, the Kruppa equation can be obtained:

$$FCF^T = \mu\left(e'\right) C \left(e'\right)^T, \tag{14}$$

where μ is an unknown proportional factor, and matrix C is a positive definite matrix.

In this paper, a sequence image matching method based on point features is proposed. The feature descriptor in SIFT (Scale Invariant Feature Transform) algorithm is introduced into image matching. In the selection of feature points, this paper uses Harris corner extraction algorithm, according to the characteristics of Harris corner, puts forward the direction feature description method of Harris corner, and introduces the feature descriptor in SIFT algorithm, which realizes the invariance of brightness, illumination and rotation in the process of image sequence matching in virtual city, and meets the needs of image matching in virtual city. The flow chart of this matching method is as follows: Figure 3.

The zoom-in and zoom-out range of buildings in the image sequence is relatively small, so we can assume that they operate on the same scale space, so we need a feature descriptor with the invariance of illumination intensity, translation and rotation, and SIFT feature descriptor has good characteristics in this respect, so this paper introduces it into the corner matching method. Harris operator principle is: if a small movement of a point in any direction will cause a great change in the gray level, then this point is a corner point. The corner response is given by eigenvalue analysis, and whether it is a corner or not is judged.

The $I(x, y)$ is used to express the intensity of gray level at point (x, y), and there is a matrix:

$$M = \begin{bmatrix} \left(\frac{\partial I}{\partial x}\right)^2 & \left(\frac{\partial I}{\partial x}\right)\left(\frac{\partial I}{\partial y}\right) \\ \left(\frac{\partial I}{\partial x}\right)\left(\frac{\partial I}{\partial y}\right) & \left(\frac{\partial I}{\partial y}\right)^2 \end{bmatrix}. \tag{15}$$

TABLE 1. Calibration results under different noise levels.

NOISE LEVEL	α	β	s	u_0	v_0
0.2	1000.769	973.6691	1.1315	428.665	374.3781
0.8	1083.7266	831.8185	1.8467	434.9505	413.1433
1.4	1143.8894	892.5527	2.153	426.9014	304.0359
2	1101.9519	797.8191	1.7054	433.7133	333.8424
2.6	1049.9946	802.8794	2.0461	421.264	351.5782
3.2	1171.3855	932.3359	1.0918	407.338	388.0441
3.8	1028.5225	834.8343	1.8443	421.9272	376.1941
4.4	1145.982	824.1695	2.161	406.9408	334.556
5	1137.7758	971.0826	1.9376	435.2033	411.2543
5.6	1067.2607	834.1319	1.442	436.5205	320.3293
6.2	990.6656	914.6412	0.8033	430.012	387.4221
6.8	1149.3689	858.7458	1.4714	409.4734	333.2252
7.4	1096.087	810.2914	2.067	403.7785	403.4863
8	1030.8149	970.9234	1.1587	415.0234	435.854

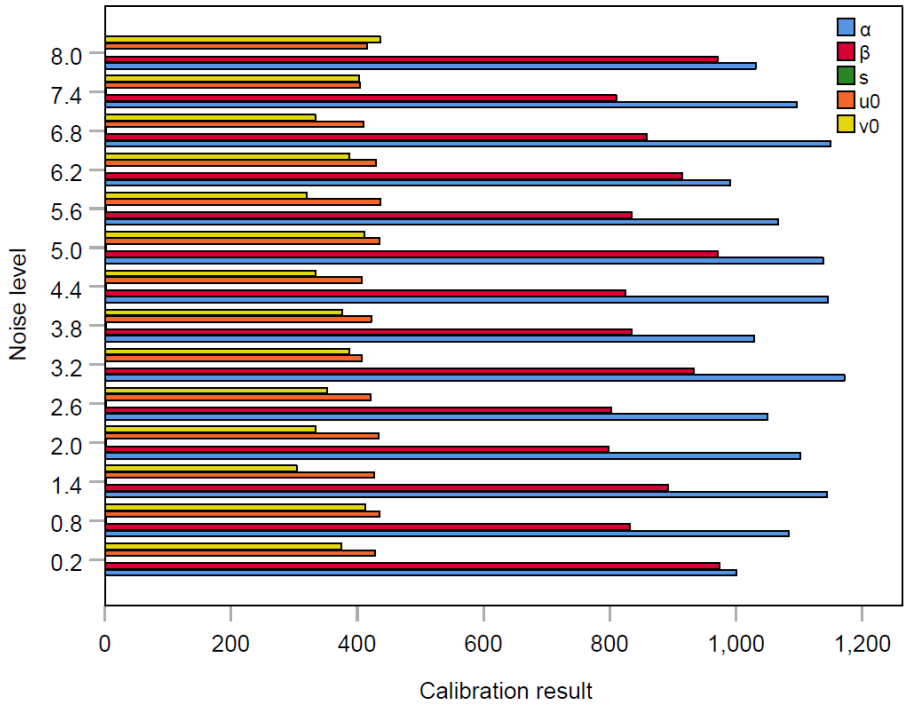

FIGURE 4. Bar chart of calibration results under different noise levels.

When both eigenvalues of the matrix M at a point are large, it means that the point is a corner point. The expression of Harris operator used in actual calculation is:

$$\Phi(x, y) = \det(M) - k(TrM)^2, \tag{16}$$

where k is an empirical value, usually 0.04-0.06. In the extraction process, a reasonable threshold T is given. When the $\Phi(x, y)$ value of a point is greater than the threshold, it means that the point is a corner point.

The most and second correlation ratio method is to find the ratio of the nearest Euclidean distance to the next nearest Euclidean distance in the matching process:

$$K = \frac{D_{nearest}}{D_{hypo-nearest}}, \tag{17}$$

where $D_{nearest}$ is the nearest European distance and $D_{hypo-nearest}$ is the next nearest European distance. If the proportional value K is greater than a certain value, it indicates that the matching point with the nearest Euclidean distance and the matching point with the next closest distance are very similar to the point to be matched, we think that this matching point pair with the nearest Euclidean distance may be a wrong match, and we will exclude this pair of matches. In this paper, we take $K = 0.7$.

IV. ANALYSIS AND DISCUSSION OF RESULTS

In the experiment, the program is used to simulate the matching points on two images from different perspectives in the same scene, and the number of matching points is. In order

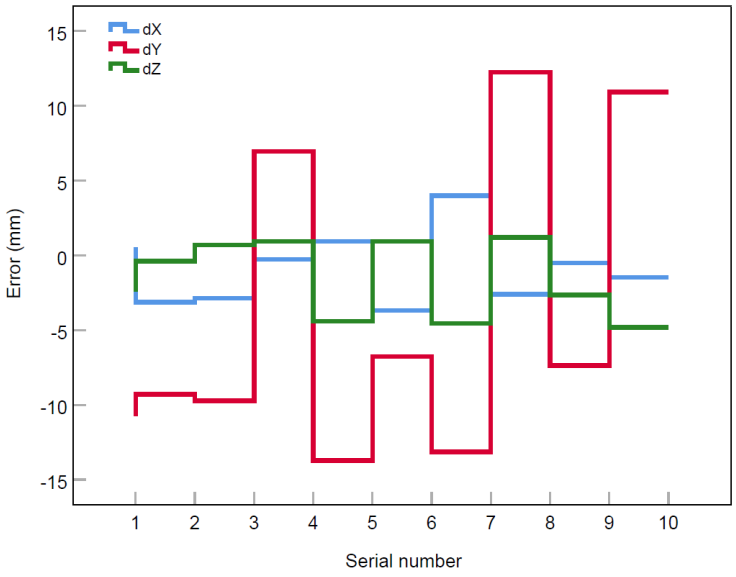

FIGURE 5. Error trend diagram.

TABLE 2. Experimental data.

SERIAL NUMBER	x	y	z	X	Y	Z
1	1046.9121	1005.2923	157.4028	36242.7053	36093.8292	40.5025
2	1052.7501	958.367	168.5552	36255.214	36130.9363	34.2263
3	994.0633	1041.1289	166.3286	36312.6975	36073.2973	34.3814
4	1034.7019	970.9962	173.4703	36220.1634	36111.7279	40.5841
5	1050.6906	1017.1797	159.8431	36279.6128	36111.7287	35.2236
6	1016.6027	1017.9021	158.1926	36341.5184	36146.3402	38.8808
7	1052.5163	1001.9679	158.3938	36231.923	36168.386	42.9073
8	1065.4222	1026.3787	159.087	36311.9923	36099.0611	34.8058
9	1058.4597	998.5748	168.3302	36235.0259	36179.4257	37.3519
10	1045.847	1032.4818	160.4884	36157.6193	36146.0046	36.6397

to simulate the matching effect of real image feature points, Gaussian noise with variance of 2 pixels is superimposed on each pair of simulated matching points. The confidence probability is 8%; Estimated data error rate = error rate of analog data +0.05. In the simulation experiment, the internal parameter of the simulation camera is $\alpha = 1100, \beta = 700, u_0 = 300, v_0 = 100, s = 0.7$, and the resolution is 1020×950.

In order to test the stability of this method in general (without excessive noise interference), Gaussian noise with a mean value of 0 and a mean square error (noise level) of 0.2 pixels to 3.0 pixels is added to the image. The relative pose with the calibration target analog camera is randomly generated within the range where the camera can see the template. Table 1 and Figure 4 show the variation of internal reference with noise obtained by simulation experiment. The nonlinear part is mainly introduced by the blue angles in the rotation matrix, which leads to the extremely complicated solution process and low accuracy. At the same time, the traditional method can only deal with the problem of small angle rotation, that is, approximate the angle transformation by Taylor formula expansion, but it is expected that there is nothing to do when facing the large angle rotation transformation.

The nonlinear problem is transformed into a linear problem, and there is no limit to the angle, which improves the efficiency and accuracy of calculation. In order to verify the effectiveness of the algorithm, we use the following data for verification (Table 2), which comes from reference [14]. In the table, the front (x, y, z) is the relative coordinates of the control points in the custom coordinate system, while (X, Y, Z) is the coordinate values of these control points in the Gaussian projection coordinate system. By substituting several parameters into the formula, the error of the algorithm can be found as shown in the following Table 3 and Figure 5.

In order to fully verify the superiority of this method, the following simulation experiments focus on comparing the VR time of 3D images of three different methods, and the specific simulation results are shown in Figure 6. The shortest image reconstruction time of this method is 4min, and the longest is no more than 6min. Because the method in this paper takes the difference degree as the constraint condition, it can effectively denoise the image, which makes the VR time of 3D image shorter, and the efficiency is obviously higher than that of the other two methods, which shows that the difference degree is of great significance to the VR of 3D image.

TABLE 3. Error statistics (mm).

SERIAL NUMBER	dX	dY	dZ
1	0.5359	-10.7529	-2.3881
2	-3.1242	-9.3052	-0.3884
3	-2.8633	-9.7379	0.7023
4	-0.2811	6.9568	0.9471
5	0.9407	-13.7321	-4.402
6	-3.6942	-6.7737	0.9274
7	3.9988	-13.1519	-4.5471
8	-2.6046	12.2407	1.1959
9	-0.5161	-7.3701	-2.6542
10	-1.479	10.9158	-4.8173

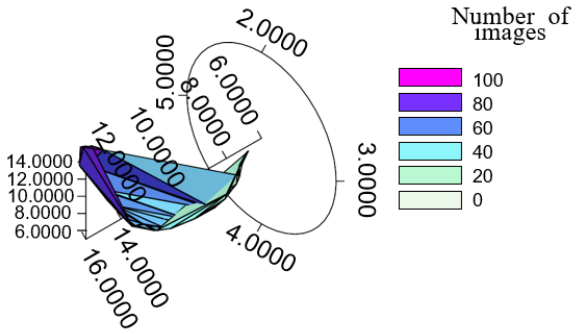

FIGURE 6. Image reconstruction time result.

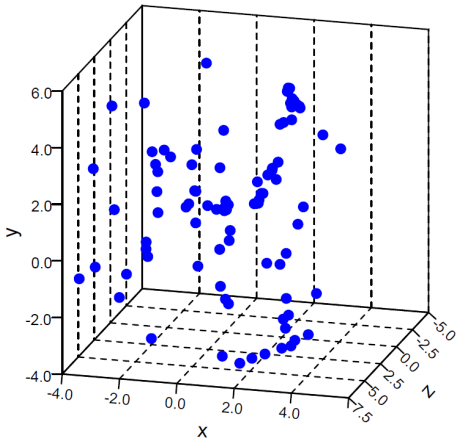

FIGURE 7. Location display of 3D points and cameras.

Setting up user's ''role'' can provide a solid foundation for the interactive framework of 3D graphical user interface. On the one hand, building roles can summarize and sort out a large amount of data from user surveys; Three aspects should be paid attention to when setting virtual user roles: First, try to make virtual roles specific, the more specific they are, the more they can play their role, and it is necessary to enrich their personality characteristics, which should be representative and also the epitome of target user characteristics; Roles should be user roles, not purchase roles. When setting virtual roles, we often put users in the role of purchase. In fact, the

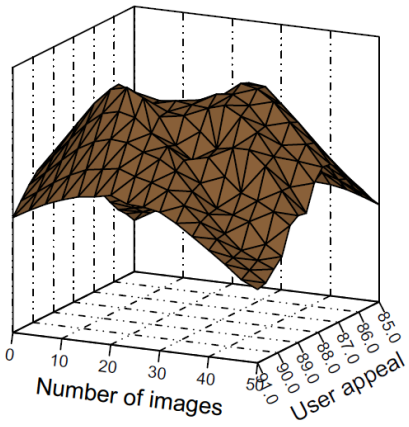

FIGURE 8. System user appeal in this paper.

purchase of 3D graphical user interface is only an intermediate link of user behavior, and its main reference purpose is to guide users when using it.

According to the image sequence, SIFT method is used to get the camera parameters and some spatial point cloud information. This method gets sparse point cloud, but when there are few images or matching points, the density of point cloud is not dense enough (as shown in Figure 7), so the reconstructed object cannot be seen, and other operations are needed to get a denser 3D point cloud. It should be noted that the 3D point position obtained by this SKF method is the information after similarity transformation. To determine its actual measurement, it is necessary to determine the similarity transformation factor.

The estimation of camera parameters is the key of 3D reconstruction. SIFT method realizes camera parameter estimation and 3D information restoration without calibration image sequence, but the camera parameters obtained by SIFT are not very ideal. Essentially, the matrix has nothing to do with the internal parameters of the camera, but only depends on the motion (translation and rotation) parameters of the camera. For experimental comparative analysis, the system in this paper and the stereo vision system proposed by ref [9] are used to reconstruct the images in 3D, and the user appeal after reconstruction is compared. The results are shown in Figure 8 and Figure 9.

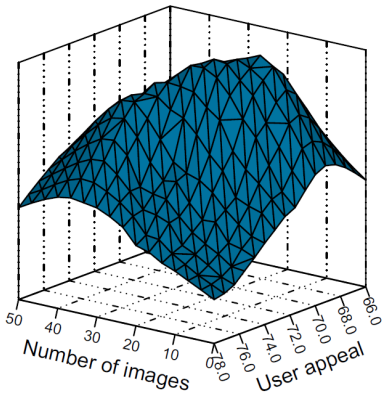

FIGURE 9. Ref [9] system user appeal.

It can be seen that in terms of user appeal, this system shows better advantages, and in terms of user appeal, this system is 12.039% higher than the comparison system. This is because the design principle of VC effect is effectively applied. The experimental results show that the system designed in this paper has good reconstruction accuracy and effectiveness. No matter how the artistic style of 3D graphical user interface design changes, the external artistic style and the connotation of the internal brand should be highly unified, so as to ensure the overall feeling of 3D graphical user interface design. Internet technology has swept the world, and the collision and blending of various new ideas and new ideas have contributed to the emergence of new concepts in the field of interface design.

The development and change of 3D graphical user interface design concepts are closely related to the development of computer design concepts, and directly lead to the reform and progress of graphical user interface design concepts. Designers are no longer limited to a certain design art style and design genre, but try to perfect an open design principle and hand over the initiative of design to the end user-users of design. The design concept of 3D graphical user interface is becoming more and more perfect and mature, and it is developing towards the ideal of ''no interface'' man-machine interface.

V. CONCLUSION

Image processing technology is widely used in various fields. With the support of computer processing technology, the optimization of images can be realized. In this paper, the research on quantitative data processing of 3D image VR algorithm based on kruppa equation in VC is carried out. A directional feature description method of Harris corner is proposed, and the feature descriptor in SIFT algorithm is introduced. Different from the existing algorithms, this algorithm only calibrates the main points of the camera, which not only makes the calibration accuracy of the main points higher, but also reduces the unknown parameters of Kruppa equation and improves the accuracy of the final calibration results. In terms of user appeal, this system shows better advantages, and in terms of user appeal, this system is 12.039% higher than the comparison system.

REFERENCES

[1] W. Wu, D. Hu, C. Niu, H. Yu, V. Vardhanabhuti, and G. Wang, ''DRONE: Dual-domain residual-based optimization network for sparse-view CT reconstruction,'' *IEEE Trans. Med. Imag.*, vol. 40, no. 11, pp. 3002–3014, Nov. 2021.

[2] W. Wu, Y. Wang, Q. Liu, G. Wang, and J. Zhang, ''Wavelet-improved score-based generative model for medical imaging,'' *IEEE Trans. Med. Imag.*, early access, Oct. 19, 2023, doi: 10.1109/tmi.2023.3325824.

[3] W. Wu, X. Guo, Y. Chen, S. Wang, and J. Chen, ''Deep embedding-attention-refinement for sparse-view CT reconstruction,'' *IEEE Trans. Instrum. Meas.*, vol. 72, pp. 1–11, 2023.

[4] M. De Paoli, S. Pirozzoli, F. Zonta, and A. Soldati, ''Strong Rayleigh–Darcy convection regime in three-dimensional porous media,'' *J. Fluid Mech.*, vol. 943, p. 51, Jul. 2022.

[5] S. Y. Chang and H.-C. Wu, ''Tensor quantization: High-dimensional data compression,'' *IEEE Trans. Circuits Syst. Video Technol.*, vol. 32, no. 8, pp. 5566–5580, Aug. 2022.

[6] J. Blumenfeld, C. Studholme, J. Carballido-Gamio, D. Carpenter, T. M. Link, and S. Majumdar, ''Three-dimensional image registration of MR proximal femur images for the analysis of trabecular bone parameters,'' *Med. Phys.*, vol. 35, no. 10, pp. 4630–4639, 2019.

[7] S. Bai, Y. Yu, W. B. Zhang, Y. Q. Mao, Y. Wang, and C. Mao, ''Three-dimensional attachment morphometry and volumetric changes of masticatory muscles after free fibular flap reconstruction of the mandibular condyle,'' *J. Cranio-Maxillofacial Surg.*, vol. 50, no. 1, p. 19–25, 2022.

[8] S. Uto, A. Hikita, T. Sakamoto, D. Mori, F. Yano, and S. Ohba, ''Ear cartilage reconstruction combining induced pluripotent stem cell-derived cartilage and three-dimensional shape-memory scaffold,'' *Tissue Eng. A*, vol. 27, pp. 604–617, May 2021.

[9] L. D. Clark, A. B. Bhagat, and S. L. Riggs, ''Extending fitts' law in three-dimensional virtual environments with current low-cost virtual reality technology,'' *Int. J. Hum.-Comput. Stud.*, vol. 139, Jul. 2020, Art. no. 102413.

[10] K. Kiraly, ''Three-dimensional virtual and printed models improve preoperative planning and promote patient-safety in complex congenital and pediatric cardiac surgery,'' *Orvosi Hetilap*, vol. 160, no. 19, pp. 747–755, 2019.

[11] W. Liu, Y. Zang, J. Qu, F. Gao, S. Zaman, G. Zhou, and S. Ji, ''Dual functions of three-dimensional hierarchical architecture on improving the rate capability and cycle performance of $LiNi_{0.8}Co_{0.1}Mn_{0.1}O_2$ cathode material for lithium-ion battery,'' *Ceram. Int.*, vol. 48, no. 7, pp. 9124–9133, Apr. 2022.

[12] C. Liu, X. Liu, Q. Tang, W. Zhou, Y. Ma, Z. Gong, J. Chen, H. Zheng, and S. W. Joo, ''Three-dimensional droplet manipulation with electrostatic levitation,'' *Anal. Chem.*, vol. 94, no. 23, pp. 8217–8225, Jun. 2022.

[13] K. W. Wong and B. Bachmann, ''Three-dimensional electron temperature measurement of inertial confinement fusion hotspots using X-ray emission tomography,'' *Rev. Sci. Instrum.*, vol. 93, no. 7, Jul. 2022, Art. no. 073501.

[14] T. El Khoury, R. Karam, E. Dib, F. Kaddah, A. Mhanna, N. Ghosn, J. Ghoubril, and E. Khoury, ''Three-dimensional comparison of the effects of sliding mechanics in labial and lingual orthodontics using the finite element method,'' *Amer. J. Orthodontics Dentofacial Orthopedics*, vol. 162, no. 1, pp. 24–32, Jul. 2022.

[15] G. Li, W. D. Zhu, H. Dong, and Y. Ke, ''Error compensation based on surface reconstruction for industrial robot on two-dimensional manifold,'' *Ind. Robot, Int. J. Robot. Res. Appl.*, vol. 49, no. 4, pp. 735–744, Jun. 2022.

[16] M. Xia, H. Yang, Y. Huang, Y. Qu, Y. Guo, G. Zhou, F. Zhang, and Y. Wang, ''AwCPM-Net: A collaborative constraint GAN for 3D coronary artery reconstruction in intravascular ultrasound sequences,'' *IEEE J. Biomed. Health Informat.*, vol. 26, no. 7, pp. 3047–3058, Jul. 2022.

[17] Y. Li, J. Gao, X. Wang, Y. Chen, and Y. He, ''Depth camera based remote three-dimensional reconstruction using incremental point cloud compression,'' *Comput. Electr. Eng.*, vol. 99, Apr. 2022, Art. no. 107767.

[18] S. Zhan and H. Zhang, ''Point cloud data processing of three-dimensional reconstruction model of object by 3D laser scanning,'' *Nonlinear Opt., Quantum Opt.*, vol. 52, pp. 205–217, Apr. 2020.

[19] C. Yuan, B. Xiong, X. Li, X. Sang, and Q. Kong, ''A novel intelligent inspection robot with deep stereo vision for three-dimensional concrete damage detection and quantification,'' *Struct. Health Monitor.*, vol. 21, no. 3, pp. 788–802, May 2022.

[20] Z. Jin, J. Cao, Y. Zhang, J. Zhou, and Q. Tian, "Novel visual and statistical image features for microblogs news verification," *IEEE Trans. Multimedia*, vol. 19, no. 3, pp. 598–608, Mar. 2017.
[21] Z. Guo, Q. Zhang, F. Ding, X. Zhu, and K. Yu, "A novel fake news detection model for context of mixed languages through multiscale transformer," *IEEE Trans. Computat. Social Syst.*, early access, Aug. 21, 2023, doi: 10.1109/TCSS.2023.3298480.
[22] X. Zhu, F. Ma, F. Ding, Z. Guo, J. Yang, and K. Yu, "A low-latency edge computation offloading scheme for trust evaluation in finance-level artificial intelligence of things," *IEEE Internet Things J.*, early access, Jul. 21, 2023, doi: 10.1109/jiot.2023.3297834.
[23] Q. Li, L. Liu, Z. Guo, P. Vijayakumar, F. Taghizadeh-Hesary, and K. Yu, "Smart assessment and forecasting framework for healthy development index in urban cities," *Cities*, vol. 131, Dec. 2022, Art. no. 103971.
[24] J. Yang, Z. Guo, J. Luo, Y. Shen, and K. Yu, "Cloud-edge-end collaborative caching based on graph learning for cyber-physical virtual reality," *IEEE Syst. J.*, vol. 17, no. 4, pp. 5097–5108, Apr. 2023, doi: 10.1109/jsyst.2023.3262255.
[25] Z. Guo, K. Yu, A. K. Bashir, D. Zhang, Y. D. Al-Otaibi, and M. Guizani, "Deep information fusion-driven POI scheduling for mobile social networks," *IEEE Netw.*, vol. 36, no. 4, pp. 210–216, Jul. 2022.
[26] D. Meng, Y. Xiao, Z. Guo, A. Jolfaei, L. Qin, X. Lu, and Q. Xiang, "A data-driven intelligent planning model for UAVs routing networks in mobile Internet of Things," *Comput. Commun.*, vol. 179, pp. 231–241, Nov. 2021.
[27] J. Yang, F. Lin, C. Chakraborty, K. Yu, Z. Guo, A.-T. Nguyen, and J. P. C. Rodrigues, "A parallel intelligence-driven resource scheduling scheme for digital twins-based intelligent vehicular systems," *IEEE Trans. Intell. Vehicles*, vol. 8, no. 4, pp. 2770–2785, Jan. 2023, doi: 10.1109/TIV.2023.3237960.
[28] J. Chen, W. Wang, B. Fang, Y. Liu, K. Yu, V. C. M. Leung, and X. Hu, "Digital twin empowered wireless healthcare monitoring for smart home," *IEEE J. Sel. Areas Commun.*, vol. 41, no. 11, pp. 3662–3676, Nov. 2023, doi: 10.1109/JSAC.2023.3310097.
[29] X. Yuan, H. Tian, Z. Zhang, Z. Zhao, L. Liu, A. K. Sangaiah, and K. Yu, "A MEC offloading strategy based on improved DQN and simulated annealing for Internet of Behavior," *ACM Trans. Sensor Netw.*, vol. 19, no. 2, pp. 1–20, May 2023.
[30] X. Yuan, Z. Zhang, C. Feng, Y. Cui, S. Garg, G. Kaddoum, and K. Yu, "A DQN-based frame aggregation and task offloading approach for edge-enabled IoMT," *IEEE Trans. Netw. Sci. Eng.*, vol. 10, no. 3, pp. 1339–1351, May 2023.
[31] Z. Guo, K. Yu, A. Jolfaei, F. Ding, and N. Zhang, "Fuz-spam: Label smoothing-based fuzzy detection of spammers in Internet of Things," *IEEE Trans. Fuzzy Syst.*, vol. 30, no. 11, pp. 4543–4554, Nov. 2022.
[32] Z. Zhou, Y. Li, J. Li, K. Yu, G. Kou, M. Wang, and B. B. Gupta, "GAN-Siamese network for cross-domain vehicle re-identification in intelligent transport systems," *IEEE Trans. Netw. Sci. Eng.*, vol. 10, no. 5, pp. 2779–2790, Sep. 2023.
[33] Z. Guo, K. Yu, K. Konstantin, S. Mumtaz, W. Wei, P. Shi, and J. P. C. Rodrigues, "Deep collaborative intelligence-driven traffic forecasting in green Internet of Vehicles," *IEEE Trans. Green Commun. Netw.*, vol. 7, no. 2, pp. 1023–1035, Jun. 2023.

QI YANG was born in Sichuan, China, in 1980. He received the bachelor's degree from Chongqing Normal University, Chongqing, in 2002, the master's degree from Peking University, in 2007, and the Ph.D. degree from Sangmyung University, South Korea, in 2022. Since 2002, he has been with Chongqing Normal University. He has published many papers, two of which has been indexed by SCI. His research interest includes digital image.

JONG HOON YANG was born in Jeju-do, South Korea, in 1961. He received the Master of Arts degree in photo communications from the University of Ohio, USA, in 1991, and the Art and Culture (Ph.D.) degree from RMIT University, Australia, in 2005. Since September 1992, he has bene with the Graduate School of Digital Image, Sangmyung University, as a Professor. His research interests include digital image and photojournalism.